METHODS

***In utero* electroporation.** Timed-pregnant ICR white mice (Charles River, E15–16) were anaesthetized with 2.5% isoflurane. The abdomen was cleaned with 70% ethanol and swabbed with iodine. A small vertical incision was made in the skin and abdominal wall and 8–12 embryos gently exposed. Each embryo was injected with 1–2 μl of DNA solution and 0.05% Fast Green[23]. pCAG-ChR2-Venus plasmid DNA was mixed with pCAG-GFP or pCAG-mRFP for a total of 1–2 μg ChR2 DNA and 0.5–1 μg of fluorophore DNA. We used a pressure-controlled bevelled glass pipette (Drummond, WPI Microbeveller) for injection. After each injection, the embryos were moistened with saline and voltage steps via tweezertrodes (BTX, 5 mm round, platinum, BTX electroporator) were applied at a zero degree angle with respect to the rostral–caudal axis of the head to target somatosensory cortex. To target cingulate cortex the polarity was reversed, and to target visual cortex the tweezertrodes were oriented 45° towards both the dorsal and caudal sides of the head. Voltage was 40 V for 5 pulses at 1 Hz, each pulse lasting 50 ms. The embryos were returned to the abdomen, which was sutured, followed by suturing of the skin. The procedure typically lasted under 20 min. On the day of birth animals were screened for location and strength of transfection by trans-cranial epifluorescence under an Olympus MVX10 fluorescence stereoscope.

Slice preparation. Cortical slices (400 μm thick, unless stated otherwise) were prepared from the transfected hemispheres of mice aged P15–P40 using a DSK Microslicer in a reduced sodium solution containing (in mM) NaCl 83, KCl 2.5, $MgSO_4$ 3.3, NaH_2PO_4 1, glucose 22, sucrose 72, $CaCl_2$ 0.5, and stored submerged at 34 °C for 30 min, then at room temperature for 1–4 h in the same solution before being transferred to a submerged recording chamber (Luigs and Neumann) maintained at 30–32 °C by inline heating in a solution containing (in mM) NaCl 119, KCl 2.5, $MgSO_4$ 1.3, NaH_2PO_4 1.3, glucose 20, $NaHCO_3$ 26, $CaCl_2$ 2.5.

For radial slices from the somatosensory barrel cortex we used the thalamocortical plane[44]; for slices from the visual or cingulate cortex we used the coronal plane; for tangential slices from the somatosensory cortex, the transfected hemisphere was trimmed on both the anterior and posterior side of barrel cortex with coronal cuts, placed on its anterior side and a cut was made with a scalpel so that much of barrel cortex lay in a plane parallel to cut. The surface of this last cut was glued to the slicer tray. The preparation was aided by the use of epifluorescent goggles to visualize the transfected area. Two to three 300–500 μm slices were prepared, the first containing much of layer 2/3 and some of layer 4. In the slices containing layer 4, barrels could be identified under the microscope by transmitted light (Supplementary Fig. 7). Digital alignment of the images of the most superficial slices with the images of deeper slices containing most of layer 4 (using vasculature landmarks and the shape) allowed post-hoc identification of the photostimulated barrel columns.

Before the beginning of the recordings, all slices were inspected with epifluorescence to ascertain the location and quality of transfection.

To test for any age-dependent effects, we split our *in vitro* results into two groups, P14–21 (group 1) and P21–28 (group 2), containing nearly all our experiments. Excitation/inhibition ratio did not differ (0.17 ± 0.04, $n = 25$ versus 0.16 ± 0.01, $n = 24$, $P = 0.89$), nor did peak oscillation frequency (30 ± 1 Hz, $n = 34$ versus 30 ± 1 Hz, $n = 16$, $P = 0.95$), nor excitatory or inhibitory power (excitation (in $pA^2\,Hz^{-1}$): $6.8 \times 10^4 \pm 8 \times 10^3$, $n = 34$ versus $9.8 \times 10^4 \pm 2.6 \times 10^4$, $n = 15$, $P = 0.24$; inhibition (in $pA^2\,Hz^{-1}$): $3.7 \times 10^5 \pm 8 \times 10^4$, $n = 30$ versus $9 \times 10^5 \pm 3 \times 10^5$, $n = 15$, $P = 0.08$). However, net excitatory and inhibitory charge during the stimulus did increase with age (excitation: 51 ± 5 pC, $n = 30$ versus 125 ± 12 pC, $n = 29$, $P < 10^{-5}$; inhibition: 410 ± 44 pC, $n = 27$ versus 804 ± 72 pC, $n = 27$, $P < 10^{-4}$). As for evoked spiking, there were no differences in the per cent suppression of layer 2/3 ($75 \pm 13\%$, $n = 5$ versus $95 \pm 3\%$, $n = 6$, $P = 0.21$) or the per cent facilitation of layer 5 ($50 \pm 32\%$, $n = 10$ versus $90 \pm 50\%$, $n = 10$, $P = 0.52$). Thus, although apparent net synaptic input increases with age in response to the same light stimulus, all other features of the observed results are the same.

Recordings *in vitro*. Whole-cell recordings were obtained with pulled patch pipettes (2–3 MΩ) containing the following caesium-based internal solution (in mM): CsMeSO-$_4$ 115, NaCl 8, HEPES 10, Na-$_3$GTP 0.3, MgATP 4, EGTA 0.3, QX-314-Cl 5, tetracaesium BAPTA 10. For current-clamp recording, K-gluconate (140 mM) was substituted for CsMeSO-$_4$, and QX-314 and BAPTA omitted. Voltage measurements were not corrected for the junction potential (8 mV established experimentally). Neurons were identified visually using oblique infrared videomicroscopy. Slices were placed in the recording chamber such that the top surface showed dendrites that were either parallel to the slice plane or such that the proximal portion of the apical dendrite was more superficial than the distal part. This ensured that recorded neurons had intact apical dendrites. Intactness of dendrites was confirmed in a subset of recordings by visualization after inclusion of Alexafluor 568 in the internal solution. We routinely used epifluorescence to either avoid recordings from transfected neurons (as for most recordings), or to target them specifically. Series resistance (ranging from 6 to 20 MΩ) was not compensated, yet monitored continuously with negative voltage steps.

Recordings *in vivo*. Electroporated mice (average P44 ± 21 (s.d.); $n = 18$) were anaesthetized with 2% isoflurane and 1.25 mg kg^{-1} chlorprothixene and attached to a head post by dental acrylic. After removal of the scalp the transfected region was identified by epifluorescence and a small craniotomy (2–2.5 mm) drilled to expose the barrel cortex.

For extracellular recording the craniotomy was covered with 1% agarose and the dura left intact. A 16-channel linear silicon electrode array (NeuroNexus Technologies, model A16 (a1x16-3mm50-177)) was inserted at a ~30° angle with respect to the brain surface, 900–1,000 μm into the cortex[45]. The isoflurane was reduced to 1% and after 30 min data were collected for 1–2 h at 1–2 recording sites. The voltage signals were amplified (16 channel amplifier AM systems) and digitized at 30 kHz (Nidaq).

For whole-cell recordings a small incision was made in the dura and recordings established by standard blind patch techniques from neurons 150–400 μm below the pia. Pipettes (2–3 MΩ) contained the caesium-based internal solution described above with the omission of QX-314 and BAPTA and the increase in CsMeSO-$_4$ to 140 mM. Following giga-seal formation and break in cells were allowed 3–5 min to stabilize and dialyse before photostimulation was commenced. For voltage-clamp recordings access resistance was 21 ± 1 MΩ ($n = 5$). For *in vivo* current clamp recordings the K^+ internal solution described above was used.

Photostimulation. For *in vitro* photostimulation a mounted 5 W blue LED (Thorlabs LEDC5) was collimated and coupled to the epifluorescence path of an Olympus BX51. All experiments were carried out under a 40× 0.8 NA water immersion lens.

For *in vivo* photostimulation a 1 mm optic fibre was coupled to a 3 W blue LED (Doric Lenses) and mounted <5 mm from the craniotomy.

Light intensity was controlled by the analogue output of an A/D card (NIDAQ, PCI6259) via a power supply (Thorlabs, LEDD1), and calibrated with photodiode and power meter. Light ramps had a duration of 1–2 s, a slope of 0.1–2.0 mW s^{-1}, started at zero intensity and reached a final intensity of 0.1–2.0 mW. The slope was adjusted for each slice to obtain a rhythmic activity with a largely stable power for the duration of the stimulus. Typically, the slope sufficient to trigger robust oscillations *in vitro* was 0.1–0.5 mW s^{-1}. The stimulus was repeated with a frequency of once a minute.

We found that careful adjustment of the light stimulus slope could induce oscillations lasting up to 30 s *in vitro* and *in vivo*. The power of activity typically decremented during the course of the stimulus probably owing to a combination of adaptive phenomena, including synaptic depression, spike after-hyperpolarization, and intrinsic desensitization of ChR2. Square light pulses lasted 5 ms at the constant power of 2 mW.

For restricted photostimulation of a circular area of ~90 μm in diameter we closed the field diaphragm of the BX51 to its minimal aperture. Microscope translation was controlled by custom routines written in Igor Pro (Wavemetrics) via the Nidaq Card and a Newport ESP600 controller. The spatial extent of neuronal recruitment by this circular photostimulus was determined as follows: we recorded from ChR2-expressing layer 2/3 pyramidal cells in the loose-patch or cell-attached configuration (Supplementary Fig. 6), and recorded the firing rate of the pyramidal cell as a function of the distance of its soma from the centre of the photostimulated area (the photostimulus was moved tangentially along the pyramidal cell layer). The firing rate of the pyramidal cells fell to $6 \pm 3\%$ ($n = 5$) of its maximal firing rate 120 μm from the centre of the photostimulated area. Thus, the circular photostimulus recruited pyramidal cells within a restricted area of approximately one barrel column in diameter (Supplementary Fig. 6). For experiments at the edge of barrel cortex, the most lateral barrel observed under the light microscope was centred and stimulation locations were at 200 μm intervals on either side of the layer 2/3 cell recorded in that barrel column.

Excitatory and inhibitory charges. Excitatory and inhibitory currents were isolated by voltage clamping the neuron at the reversal potential for synaptic inhibition and excitation respectively. The current was integrated over a 1 s period from the onset of the light ramp. For oscillations initiated *in vitro* the net excitatory charge averaged (in pC): L2/3, 87 ± 7, $n = 58$; L4, 4 ± 1, $n = 16$; L5, 107 ± 14, $n = 34$; L6, 4 ± 1, $n = 15$. The excitatory power between 20–60 Hz averaged (in 10^3 $pA^2\,Hz^{-1}$): L2/3, 1.7 ± 0.6, $n = 46$; L4, 0.014 ± 0.004, $n = 15$; L5, 2.5 ± 0.9, $n = 20$; L6, 0.03 ± 0.02, $n = 14$. The net inhibitory charge averaged (in pC): L2/3, 605 ± 50, $n = 53$; L4, 16 ± 4, $n = 16$; L5, 540 ± 70, $n = 32$; L6, 10 ± 2, $n = 13$. The inhibitory power between 20–60 Hz averaged (in 10^4 $pA^2\,Hz^{-1}$): L2/3, 4 ± 1; L4, 0.03 ± 0.01; L5, 4 ± 1; L6, 0.03 ± 0.02. These data

are averaged across all simultaneous dual and quadruple recordings (Fig. 2b). For simultaneous recordings of layer 5A and layer 5B pyramidal cells, the excitatory charge averaged (in pC): L5A, 58 ± 10; L5B, 104 ± 58, $n = 11$. The excitatory power between 20–60 Hz averaged (in 10^3 pA^2 Hz^{-1}): L5A, 2.2 ± 0.9; L5B, 6 ± 1, $n = 11$. The inhibitory charge averaged (in pC): L5A, 230 ± 40; L5B, 360 ± 80, $n = 11$. The inhibitory power between 20–60 Hz averaged (in 10^4 pA^2 Hz^{-1}): L5A, 2.0 ± 0.9; L5B, 8 ± 2, $n = 11$ (Supplementary Fig. 5).

Data acquisition and analysis. *In vitro* data were recorded with Multiclamp 700B amplifiers (Axon instruments) filtered at 2 kHz and digitized with a Nidaq Card at 10 kHz. Data *in vivo* were recorded with Axopatch 200A (Axon instruments) filtered at 2 kHz and digitized with a Nidaq Card at 10 kHz. For multichannel recording an AM systems 16-channel model 3500 amplifier was used, filtered at 0.3–5,000 Hz and digitized at 30 kHz.

All data acquisition, analogue output control and analysis were performed by custom routines written in Igor Pro (Wavemetrics). Average values are expressed as means ± s.e.m. The student *t*-test, paired *t*-test, one-way ANOVA and Kolmogorov–Smirnov tests were used for statistical comparisons, as indicated in the results. Drugs used were NBQX, CPP and SR95531 (gabazine) (Tocris Cookson).

To measure the speed of propagation of the oscillation we simultaneously recorded from pairs of layer 2/3 cells either immediately next to each other, or 300–400 μm apart, and focally stimulated with light ramps as described above. We then computed the cross-correlation of their rhythmic excitatory or inhibitory inputs and divided the lag of the peak of the cross-correlogram by their inter-somatic distance. Neighbouring cells had a lag of 0.26 ± 0.15 ms ($n = 3$) whereas separated cells had a lag of 1.7 ± 0.3 ms ($n = 6$, $P = 0.004$).

Bypassing axons expressing ChR2 do not contribute to oscillatory activity. Photoinitiated gamma activity necessitated an intact somatodendritic compartment of ChR2-expressing pyramidal cells, as light-ramp photostimulation of cortical areas containing only ChR2-expressing axons (for example, layer 5; Supplementary Fig. 6), although transiently inducing some transmitter release (only 5 ± 2% of the charge as compared to stimulation on layer 2/3 in the same slices), did not lead to gamma oscillations. Thus, whereas strong light pulses can directly evoke release from ChR2-expressing axons[24,25], at the intensities used to evoke gamma oscillations in this study, rhythmic release from directly stimulated axons was negligible.

Replay of synaptic currents. Layer 2/3 and Layer 5 pyramidal cells were patched with two pipettes at the soma in the current clamp configuration, one to impose an inhibitory conductance, the other to inject an excitatory current. The inhibitory conductance waveform had the amplitude and time course of an inhibitory conductance recorded at the soma of either a layer 2/3 or a layer 5 pyramidal cell during photoinduced oscillations. The waveforms were taken from pairs of simultaneously recorded layer 2/3 or layer 5 cells where one cell was held at EPSC reversal and the other at IPSC reversal to preserve the relative temporal relationship of the two conductances. Additionally, their excitation and inhibition ratio approximated the mean measured from our sample of simultaneously recorded layer 2/3 and layer 5 cells.

To impose the inhibitory conductance (dynamic clamp), the external command of the amplifier connected to one of the pipettes was controlled such as to inject a current that was, at any time point, equal to the conductance times the difference between the membrane potential of the neuron and the reversal potential for inhibition, set at −60 mV. The operation was performed by a custom-made analogue circuit (5 MHz bandwidth) receiving an input from the amplifier for the membrane potential of the neuron, an analogue input for the conductance waveform, and sending an output to the external command of the amplifier to control the current injected into the neuron.

The excitatory input was simulated by directly injecting, through the other pipette, excitatory current waveforms recorded during photoinduced oscillations at the soma of either a layer 2/3 or a layer 5 pyramidal cell voltage clamped at −70 mV.

In each experiment a square depolarizing current step was first injected alone to elicit baseline firing at 3–9 Hz (Fig. 5c, left), this current step was then delivered again together with the excitatory and inhibitory waveforms (Fig. 5c, middle and right).

We tested the impact of excitatory and inhibitory waveforms on spike rate modulation by re-injecting these waveforms in the soma despite the fact that excitatory and inhibitory synaptic inputs are distributed along the somatodendritic axis pyramidal cells. We reasoned that because in pyramidal cells the axon initial segment, where action potentials are initiated[35,36,46], originates from the soma, the waveform that matters in terms of spike rate modulation is the one recorded at the soma. Simply stated, injecting a waveform in the soma should reproduce the original somatic membrane potential trajectory as long as what is injected in the soma is what is recorded at the soma. We have ascertained the accuracy of this hypothesis using a simple ball-stick simulation of a neuron implemented in the NEURON environment[47]. We compared the somatic membrane potential fluctuation of the model neuron in response to the following two conditions: (1) a simulated excitatory synaptic conductance into the dendrite; (2) somatic injection of the excitatory waveform obtained under somatic voltage clamp in response to the same dendritic conductance injection. Consistent with imperfect space clamp, the conductance obtained under somatic voltage clamp was (relative to the conductance at its site of origin in the dendrites) diminished in amplitude, temporally filtered, and had an apparent reversal potential above 0 mV; that is, above the reversal potential of the excitatory conductance at its site of origin. However, re-injecting this waveform into the soma generated a somatic membrane potential trajectory that was identical to that obtained in response to the dendritic conductance. Thus, our somatic replay of somatically recorded waveforms probably closely reproduces the somatic membrane potential fluctuations experienced by pyramidal cells in response to spatially distributed synaptic inputs.

45. Niell, C. M. & Stryker, M. P. Highly selective receptive fields in mouse visual cortex. *J. Neurosci.* **28,** 7520–7536 (2008).
46. Palmer, L. M. & Stuart, G. J. Site of action potential initiation in layer 5 pyramidal neurons. *J. Neurosci.* **26,** 1854–1863 (2006).
47. Carnevale, N. T. & Hines, M. L. *The NEURON Book* (Cambridge Univ. Press, 2006).

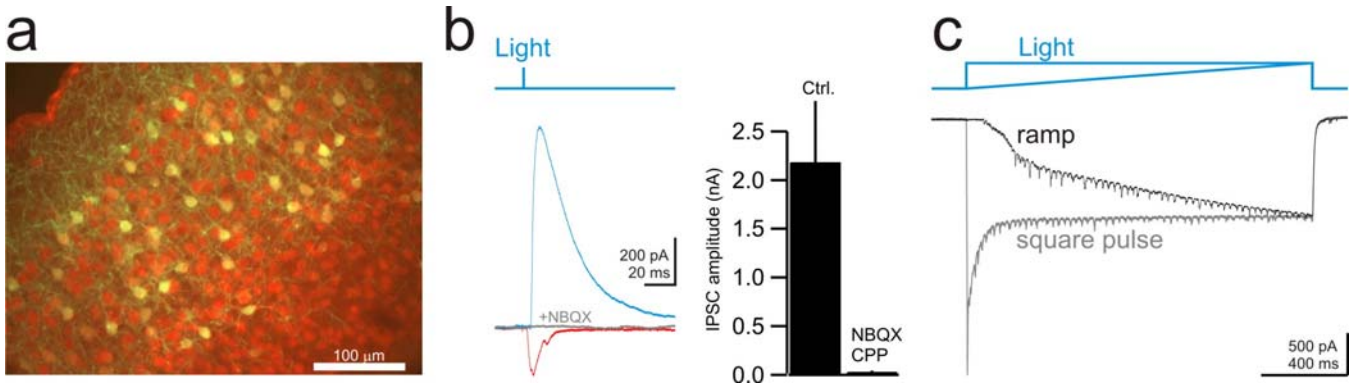

Supplemental Figure 1: Selective expression of ChR2 in layer 2/3 excitatory neurons and photo-currents. **a,** Left: Section of *in utero* electroporated mouse brain (P60) expressing ChR2 and GFP (and immunostained for GFP). Overlay of green channel (GFP, $ChR2^{+}$ cells) and red channel, anti-NeuN, to stain all neurons. **b,** Left: synaptic response to a pulse of blue light (1 ms, 2 mW) recorded in a $ChR2^{-}$ layer 2/3 PC *in vitro,* voltage clamped -70 mV (red, EPSC) and +10 mV (blue, IPSC). Following application of the AMPA receptor antagonist NBQX (10 µM; gray) the IPSC is abolished, indicating the lack of ChR2 expression in GABAergic interneurons. Right: average reduction in IPSC amplitude in NBQX and CPP, an NMDA receptor antagonist (5 µM and 10 µM respectively; 99±1% reduction, n = 12, p = 0.005). Error bars are ±s.e.m. **c,** Comparison of a photo-current evoked in a $ChR2^{+}$ layer 2/3 PC (V_h=-70 mV) by a 2 second-long low-intensity pulse (gray) or ramp (black) of blue light. Both stimuli had the same final intensity (0.15 mW).

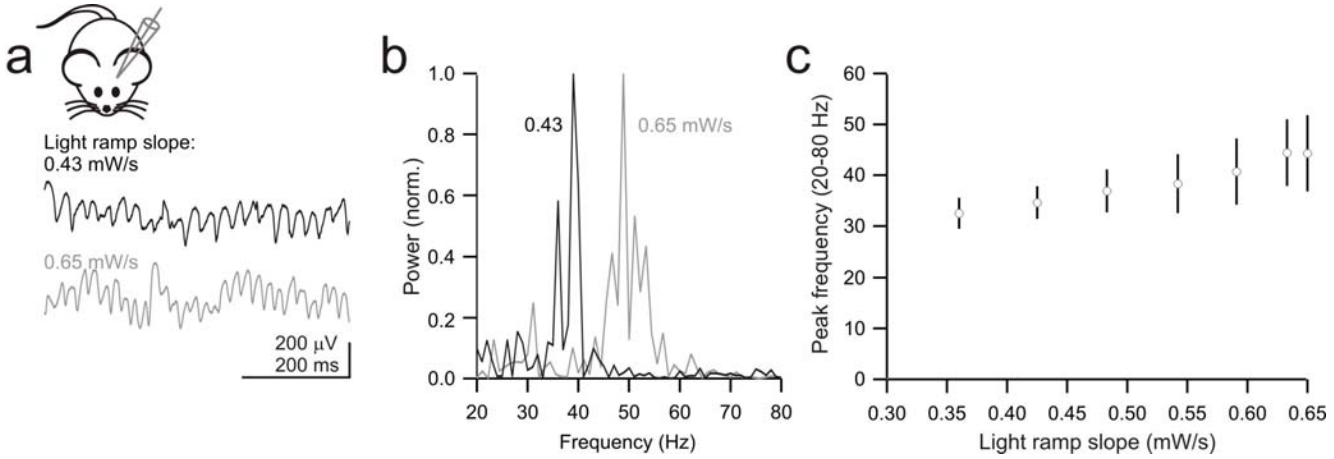

Supplemental Figure 2: Dependence of the oscillation frequency on the slope of the photo-stimulus *in vivo*. **a,** *In vivo* LFP (band pass filtered between 1-100 Hz) recording from layer 2/3 in response to a photo-stimulus whose slope was just slightly steeper than what sufficient to elicit an oscillation (0.43 mW/s; black) or in response to a photo-stimulus that triggered the maximal oscillation frequency (0.65 mW/s; gray). **b,** Normalized power spectra of the response to the two photo-stimuli. Note the shift in frequency. **c,** Plot of the peak frequency (between 20-80 Hz) against photo-stimulus slope for 5 similar experiments. Error bars are ±s.e.m.

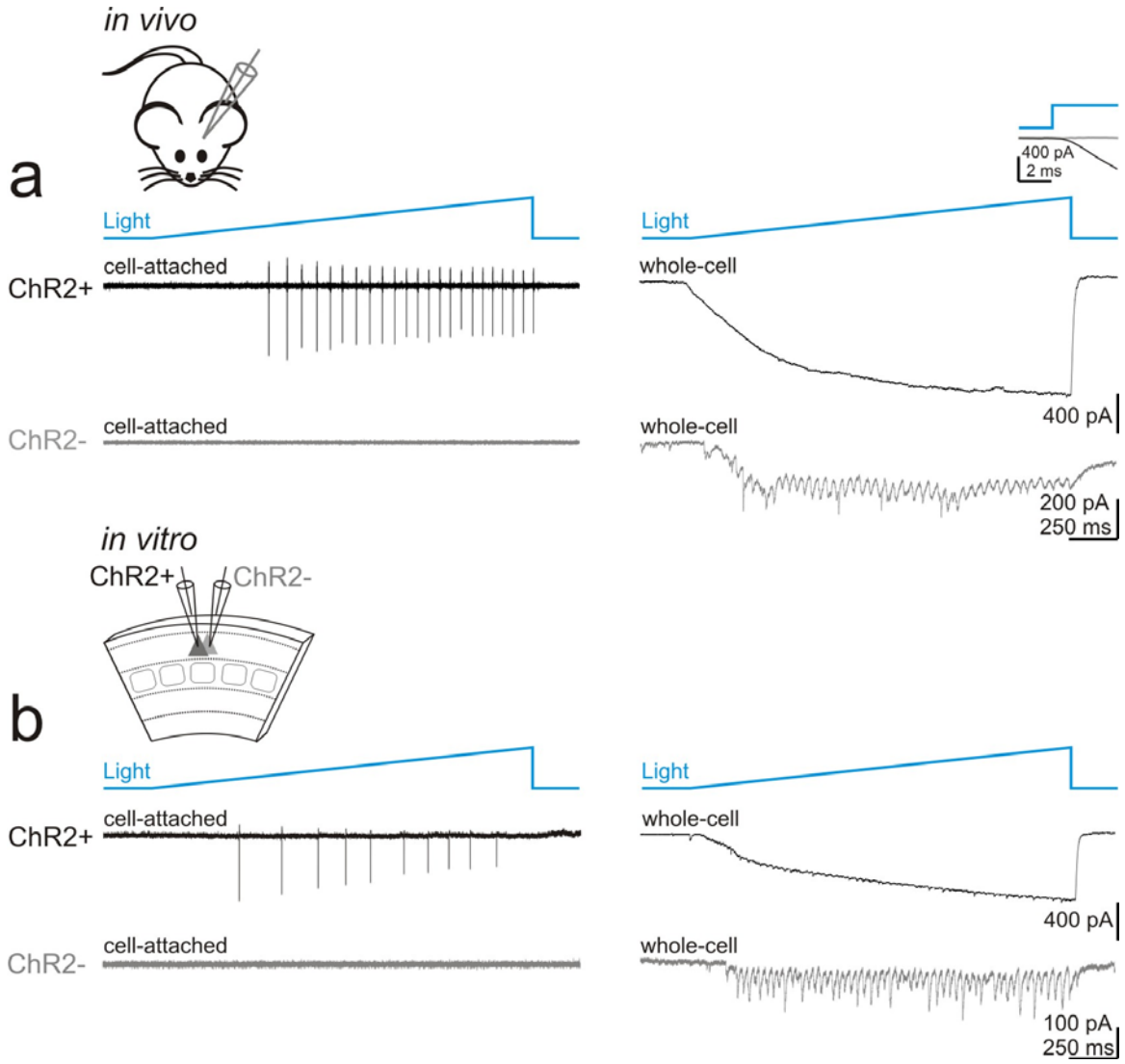

Supplemental Figure 3: Cellular response of $ChR2^+$ and $ChR2^-$ layer 2/3 PCs during oscillatory activity *in vivo* and *in vitro*. **a,** Left: Cell-attached *in vivo* recordings from $ChR2^+$ (top, black) and $ChR2^-$ (grey) layer 2/3 PCs during light ramps. Note the spiking of the $ChR2^+$ PC. Right: whole cell voltage clamp records from the same cells shown at left, confirming the presence (top) or absence (bottom) of a direct ChR2-mediated photocurrent Inset: Membrane current response to a square pulse of light in the $ChR2^+$ (black) and $ChR2^-$ (grey) cell at the onset of light before the beginning of a synaptic response demonstrates a direct photocurrent in the $ChR2^+$ cell, but no photocurrent in the $ChR2^-$ cell. **b,** Left: Simultaneous *in vitro* cell-attached recordings from a $ChR2^+$ (top, black) and a $ChR2^-$ (bottom, gray) layer 2/3 PC during photo-stimulation (top, blue). Note the spiking of the $ChR2^+$ PC. Right: Simultaneous whole cell voltage clamp recording PC (V_h=-70 mV) from the same two PCs illustrating the presence (top, black) and absence (bottom, gray) of photocurrent.

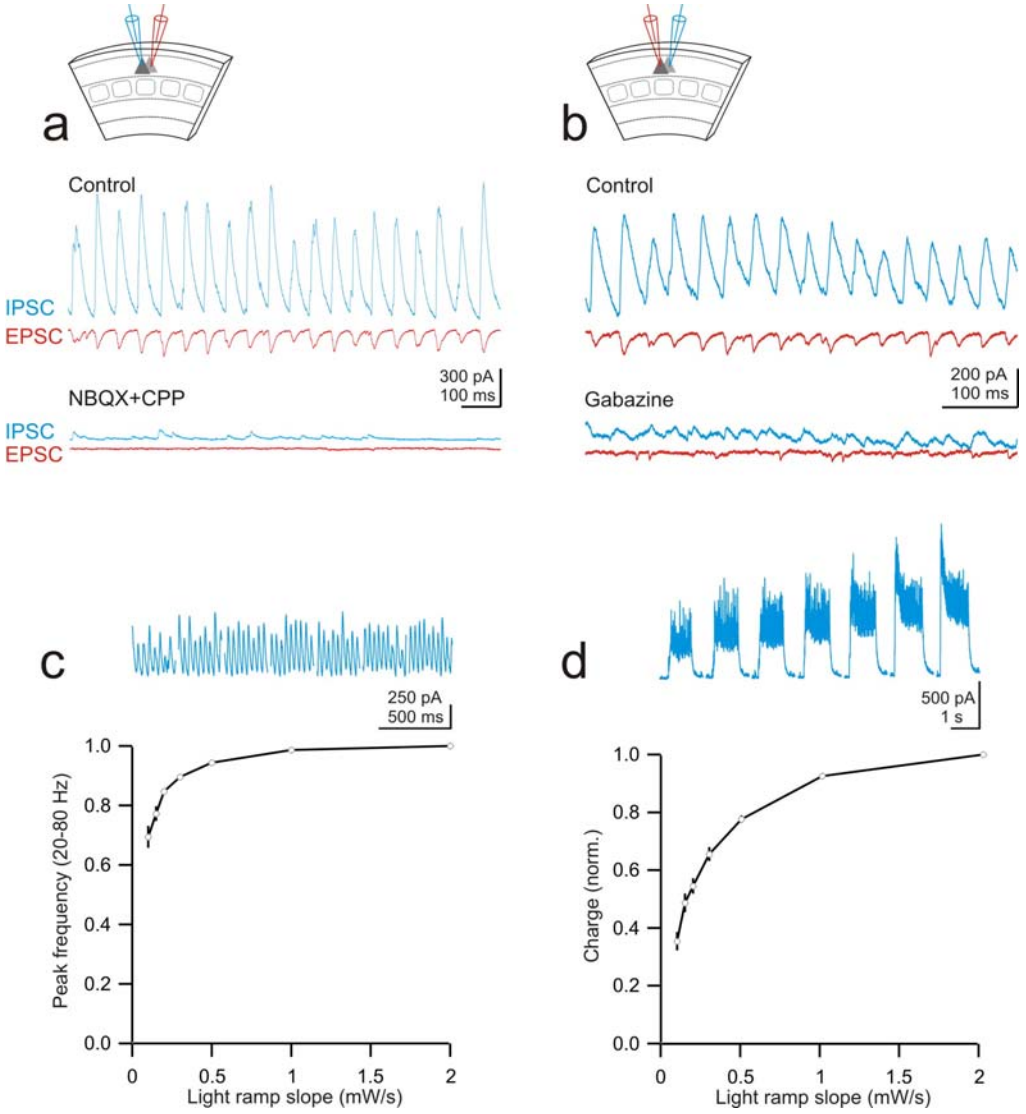

Supplemental Figure 4: Dependence of light-induced oscillations on excitatory and inhibitory transmission and slope of the photo-stimulus. **a,** Simultaneous recordings from two layer 2/3 PCs during light ramp induced oscillations. The oscillations of both IPSCs (blue, recorded at +10 mV) and EPSCs (red, recorded at -70 mV) are abolished by the AMPA and NMDA receptor antagonists NBQX (5 μM) and CPP (10 μM). **b,** As in a, different slice. The oscillations are abolished by sub-saturating concentrations of the $GABA_A$ receptor antagonist gabazine (400 nM; average reduction in excitation: Power: 88±2% reduction, p = 0.00005; charge: 46±7% reduction, n = 11, p = 0.009). **c,** Plot of the IPSC frequency (normalized for maximal frequency) against the slope of the light ramp (n=10). The shallowest slope was just sufficient to trigger an oscillation. The blue traces on top illustrate IPSC oscillations recorded in one layer 2/3 PC in response to seven different light ramp slopes of increasing steepness (from left to right). **d,** Plot of IPSC charge transfer (normalized by maximum charge transfer) against the slope of the light ramp (n=10). The blue traces on top illustrate IPSC oscillations recorded in one layer 2/3 PC in response to seven different light ramp slopes of increasing steepness (from left to right). Error bars are ±s.e.m.

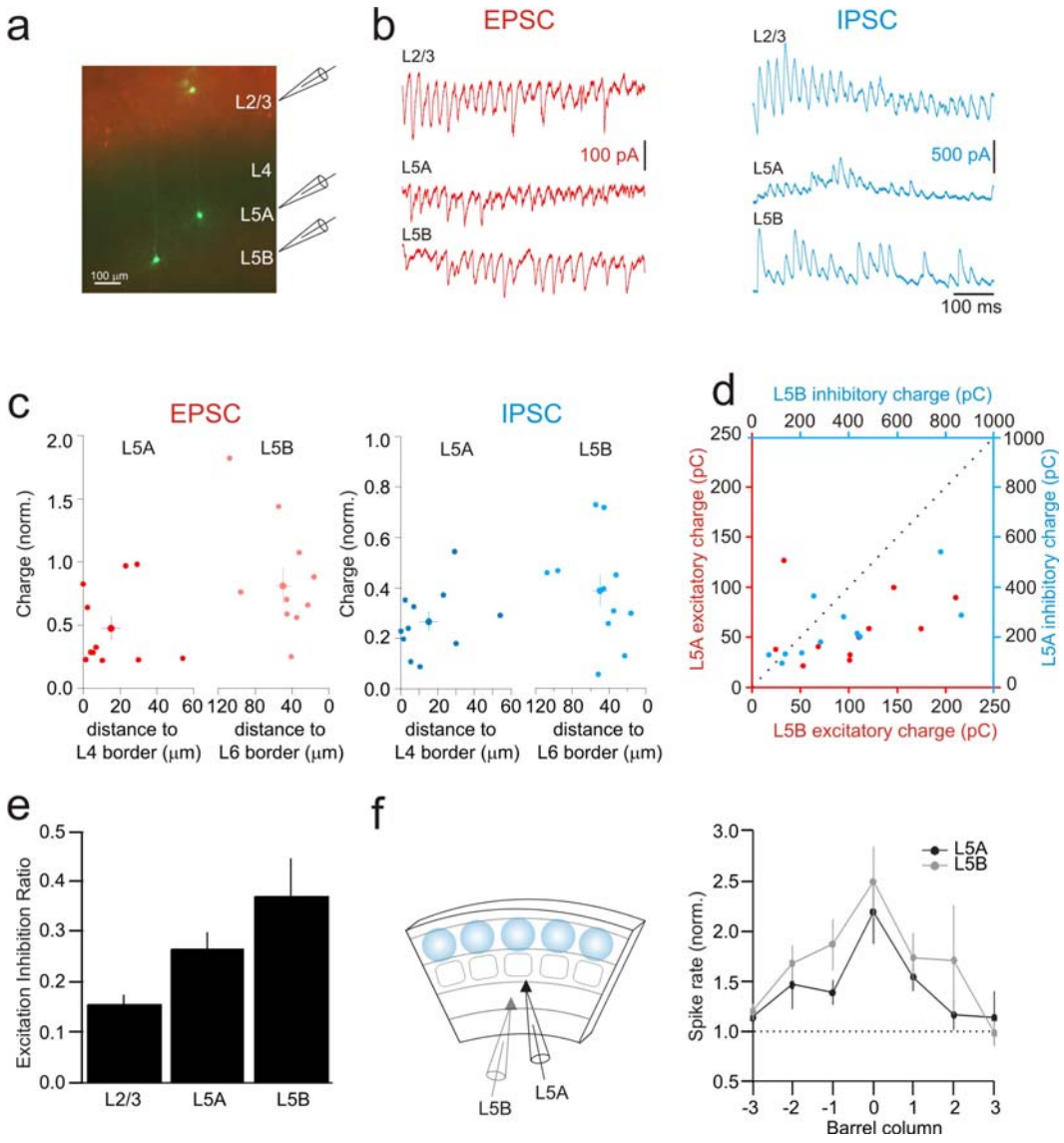

Supplemental Figure 5. Comparison between Layer 5A and Layer 5B PCs. **a,** Image of a slice in which a layer 2/3, a layer 5A, and a layer 5B PC were simultaneously recorded and filled with Alexafluor 488. **b,** left: EPSC waveforms recorded simultaneously in L2/3, L5A and L5B PCs during photo-generated oscillations. Right: IPSC waveforms recorded in the same cells. **c,** Left: scatter plot of normalized excitatory charge in layer 5A PCs (red) and in layer 5B PCs (pink) versus distance from layer 4/5 or layer 5/6 border, respectively ($n = 11$, $p < 0.05$, see methods; the charge is normalized by the excitatory charge simultaneously recorded in L2/3 PCs). Right: similar scatter plot for normalized inhibitory charge ($n = 11$, $p < 0.05$). **d,** Scatter plot of excitatory (red) and inhibitory (blue) charge between pairs of simultaneously recorded layer 5A and layer 5B PCs ($n = 11$ pairs). Note that data points tend to be below the unity line (dashed) indicating larger charges in layer 5B PCs. **e,** Bar graph of average excitation/inhibition ratios between layer 2/3, layer 5A, and layer 5B PCs (triple recordings, excitation-inhibition ratio significantly larger in L5A and L5B compared L2/3; $p < 0.05$; excitation-inhibition ratio not significantly different between L5A and L5B, $p = 0.13$; $n = 11$). **f,** Left: Schematic of photo-stimulation and recording configuration. Right: Change in spike rate of layer 5A (black; n=8) and layer 5B (gray; n=7) PCs plotted against barrel-column distance from focal light stimulation ($p = 0.54$ at the home barrel column).

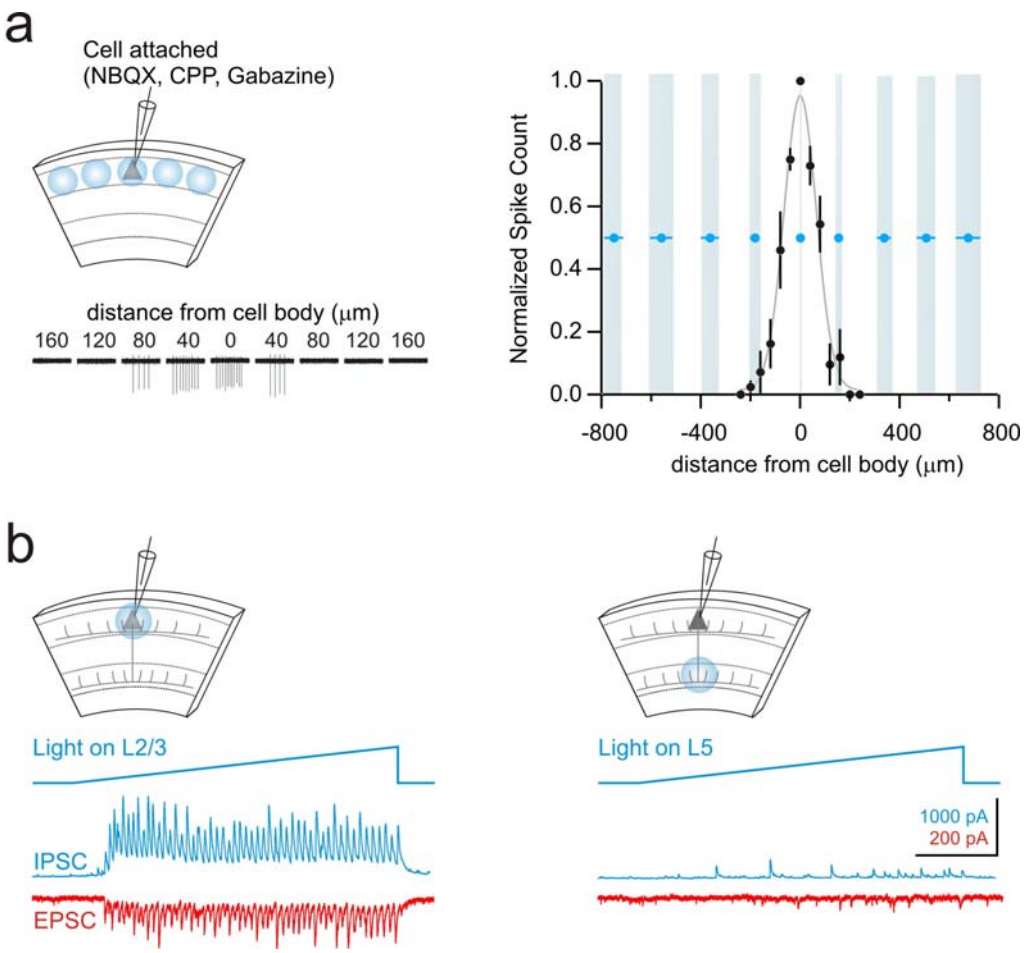

Supplemental Figure 6: Focal photo-stimulation permits spatially confined activation of ChR2$^+$ layer 2/3 PCs and avoids direct activation of ChR2$^+$ fibers of passage. **a,** Direct activation of ChR2$^+$ PCs as measured in the cell-attached mode by a circular photo-stimulus of 90 μm diameter in the presence of blockers of synaptic transmission (NBQX, CPP 5 μM and 10 μM,). Left: Example traces of light-evoked action potentials recorded in the cell-attached configuration of a ChR2$^+$ PC as the focal photo-stimulus was translated laterally across layer 2/3 (distance from the cell indicated above each trace; see methods for details). Right: Average spatial profile of light evoked firing across multiple ChR2$^+$ PCs (black dots, n = 5). Overlaid on the graph is the average locations of barrel columns measured in the slices used for experiments in Figure 3 (blue dots and bars). Error bars are ±s.e.m. **b,** Oscillations can only be evoked when the light stimulus activates the somato-dendritic compartment of ChR2$^+$ layer 2/3 cells. Response to light ramp recorded in a ChR2$^-$ PC (EPSC, red; IPSC blue) when the light stimulus was located on layer 2/3 (left; to activate the somato-dendritic compartment) and layer 5 (right; to activate layer 2/3 PC axons only). Note that oscillations are induced only when the light ramp is located on layer 2/3 and not layer 5; when the photo-stimulus was on layer 5 the average power (between 20-60Hz) was only 1.0±0.8% (n = 8 p=0.03) of the power elicited by a stimulus on layer 2/3: the average charge was only 5±2%; (n = 8; 0.01; see methods for details).

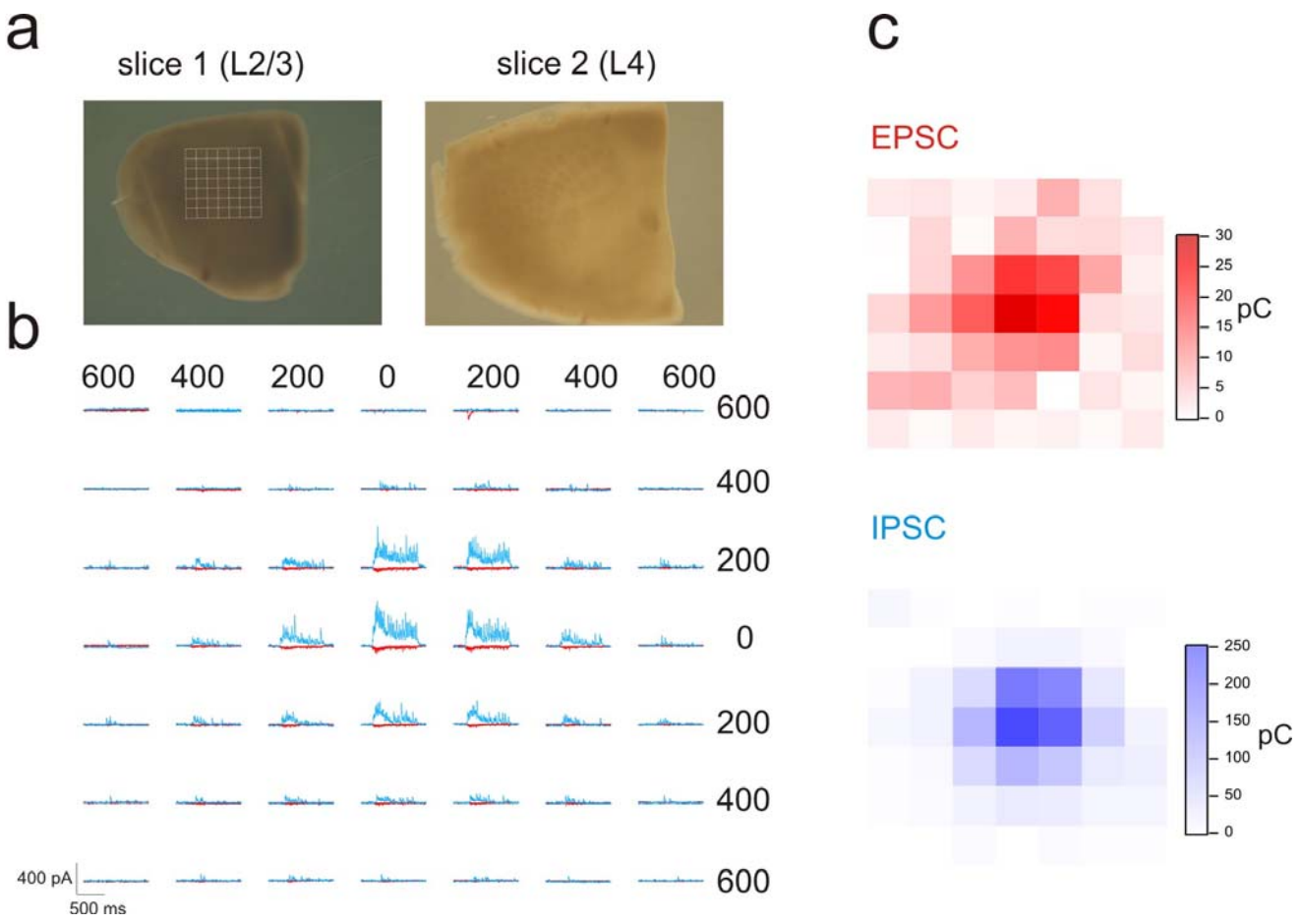

Supplemental Figure 7: Spatial decay of oscillatory input in tangential Slices.
a, Left: bright field image of the top-most tangential slice containing layer 2/3 in which cells were recorded. The white overlaid grid represents the stimulation locations. Right: Bright field image of the second tangential slice containing the barrels of layer 4 which were use to determine the spatial locations of stimulation post hoc. **b,** Traces of excitatory (red) and inhibitory (blue) input to the recorded layer 2/3 cell for focal light stimulation at 200 µm intervals in two dimensions. Numbers indicate distance in microns from the recorded neuron. **c,** Top: Two dimensional (left) and color-coded plots of evoked excitatory charge for the same cell as in **b**. Bottom: Similar plot for evoked inhibitory charge (n = 4).